Influence of the Pacific-South American Modes and Other Climate Modes on the Global Spectral Wind-wave Climate

E. R. Echevarria[1,2,3], M. A. Hemer[1], N. J. Holbrook[2,3] and A. G. Marshall[3,4]

[1]CSIRO Oceans and Atmosphere, Hobart, Tasmania, Australia

[2]Institute for Marine and Antarctic Studies, University of Tasmania, Hobart, Tasmania, Australia

[3]Australian Research Council Centre of Excellence for Climate Extremes, University of Tasmania, Hobart, Tasmania, Australia

[4]Buerau of Meteorology, Hobart, Tasmania, Australia

Corresponding author: Emilio Echevarria (emilio.echevarria@csiro.au)

Key Points:

The influence of the Pacific South American (PSA) modes on the global spectral wind-wave climate is analysed

The PSA modes are significantly correlated with the variability of modelled wave heights and directions in the south Pacific

Composite wind anomalies for positive stages of PSA modes are shown to explain the observed correlation patterns

Abstract

In this study, we analyse the influence of the Pacific South American modes (PSA-1 and PSA-2) on the global wind-wave climate using wave data derived from a WAVEWATCH III global wave hindcast. We apply an empirical orthogonal function analysis to daily-averaged directional wave spectra to extract the two main patterns of interannual wave spectral variability. These are related to changes in the wave spectral density levels (variability in the wave heights) and to rotations of the wave signal (variability in wave direction). The PSA-1 mode is positively correlated with the wave height variability in the southeast Pacific, and negatively correlated in the Indian Ocean sector of the Southern Ocean. The PSA-2 mode presents a strong and negative correlation with wave heights in the central South Pacific. Moreover, the PSA modes are significantly correlated with changes in modelled wave direction in the South Pacific region. Composite maps of wind anomalies during positive stages of PSA-1 and PSA-2 modes provide a compelling explanation for the observed correlation patterns. The methodology applied in this study is also used to assess the influence of other climate modes on the global wind-wave climate (namely, the Southern Annular Mode, Artic Oscillation, North Atlantic Oscillation, El Niño/Southern Oscillation and the Pacific North American mode). While our results are consistent with previous studies, we provide more clarity as to how different atmospheric modes influence the variability of specific components of the wave spectrum.

Plain Language Summary

Different modes of atmospheric variability (such as El Niño/Southern Oscillation or the Southern Annular Mode) are known to influence the ocean wind-wave climate in many regions of the world and across different timescales. The Pacific South American (PSA) patterns represent important modes of variability of the atmospheric circulation in the Southern

Hemisphere. In this study we use results from an ocean wind-wave model to analyse how the PSA patterns influence the global wave field. We apply a methodology that allow us to study in detail changes in wave height and direction. Our results suggest that the PSA modes would be associated with wind anomalies that modulate the height and direction of swell waves generated in the Southern Ocean, particularly in the south Pacific. We also analyse other climate modes of variability and their influence on the wind-wave field. Our results are consistent with previous studies, and they suggest that the influence of the PSA modes on the wind-wave field is of the same order of magnitude as that of other climate modes.

1 Introduction

The wind-wave state of a given region can change in a matter of hours, but also across timescales from daily to interannual and longer. It is important to understand the nature of these variations to improve wave climate predictability and to provide a context to the study of wave trends and extreme values. The question of what drives interannual variability in the global wave field has been explored in several studies, and this knowledge has improved greatly in recent years, given the increasingly long record of wave observations (obtained remotely by satellites and in situ from buoys) and the development of global wind-wave model hindcasts and reanalyses. Large-scale modes of climate variability, such as El Niño – Southern Oscillation (ENSO), the Southern Annular Mode (SAM) and the Arctic Oscillation (AO), among others, are known to modulate interannual variations in surface winds and have an important influence on the global surface ocean wave climate (e.g., Hemer et al., 2009; Izaguirre et al., 2011; Marshall et al., 2015; Marshall et al., 2018; Marshall et al., 2020; Shimura et al., 2013; Stopa et al., 2013).

The Pacific-South American (PSA) modes represent one of the dominant atmospheric circulation features in the Southern Hemisphere. First identified by Mo and Ghil (1987), the

PSA is identified as an atmospheric Rossby wave train extending from south-eastern Australia to Argentina. It is analogous to the Pacific-North American pattern (Wallace and Gutzler, 1981), hence its name. However, the PSA modes (or patterns) are defined with two patterns instead of one, namely PSA-1 and PSA-2. They are usually defined as the second and third empirical orthogonal functions (EOFs) of 500-hPa geopotential height (or 200-hPa streamfunction) monthly anomalies in the Southern Hemisphere, while the first EOF mode corresponds to the SAM. Importantly, the PSA-1 and PSA-2 modes are in quadrature and together depict the wave train. They are dominated by wavenumber 3 in midlatitudes, with largest amplitudes in the geopotential height field in the South Pacific sector of the Southern Ocean (Figure 1), and centers at approximately 60°S; 120°W (PSA-1) and 60°S; 90°W (PSA-2). They manifest in the intra-seasonal to decadal time scales. It has been shown that the PSA patterns play a significant role in atmospheric blocking events (Renwick and Revell, 1999) and in South American rainfall variability (Mo and Paegle, 2001). Importantly, they have been linked to the warming observed over West Antarctica and the Antarctic Peninsula (Marshall and Thompson, 2016) and to Antarctic precipitation variability (Marshall et al., 2017). Being such an important source of atmospheric circulation variability, the PSA patterns presumably exert a significant influence on the surface winds, and consequently, on the wind-wave climate of the South Pacific Ocean. However, this link has not yet been explored nor quantified. This paper aims to assess the influence of the PSA patterns, as well as other known large-scale climate modes, on the global wind-wave climate on interannual time scales together with their potential consequences. A global wind-wave hindcast, together with an atmospheric reanalysis, are used to accomplish this.

Usually wave studies employ integrated parameters, such as significant wave height (Hs), mean period (Tm) or mean direction (θm). These values are computed through an integration of the wave spectrum, with the objective of reducing the information to a set of parameters (Hs, Tm,

θm) that are representative of the average bulk wave climate. On the other hand, a directional wave spectrum describes how the waves' energy is distributed across frequencies and directions, hence providing the most complete description of the wave climate in a certain region, since it characterizes all the wave modes that may be present. Several authors (e.g., Echevarria et al., 2019; Hegermiller et al., 2017; Portilla-Yandún et al., 2016; Portilla-Yandún 2018) outlined potential problems that could arise when describing the wave climate with integrated parameters. For example, defining the peak direction in a case with two independent swell modes will only consider the most energetic one and disregard the other. Considering the mean swell direction in the presence of opposing swell waves will not faithfully represent any of the wave components: for example, having two swell systems propagating to the southeast and northeast could yield an average direction to the east. This case may arise in the equatorial Pacific which receives swell waves from high latitudes of both hemispheres (Echevarria et al., 2019; Semedo et al., 2011; Young 1999). Likewise, the estimation of other wave parameters will be affected. Moreover, Portilla-Yandún et al. (2016) and Portilla-Yandún (2018) found that the presence of multiple swells and wind sea is rather common in most ocean basins. These findings motivated us to employ an approach for the description of the wave climate that considers all the possible wave modes. As will be described in Section 2.2, the methodology devised in Echevarria et al. (2019) was implemented to obtain the main patterns of wave spectral variability on interannual time scales and then assess the influence of large-scale atmospheric forcing contributions associated with various climate modes on them. This work can be regarded as a continuation of the study by Echevarria et al. (2019), extending the methodology from investigating seasonal variability of the spectral wave climate to considering interannual timescales of variability.

This paper is organized as follows: Section 2 describes the wave hindcast data and the methodology to extract the patterns of spectral variability; it also defines and describes the PSA

patterns and indices. Section 3 accounts for the results, showing the two main patterns of spectral variability at each grid point and their relationship to the PSA patterns and other climate modes. Finally, a summary and discussion of the main outcomes are presented in Section 4.

2 Data and Methods

2.1 The CAWCR waves hindcast

The Centre for Australian Weather and Climate Research (CAWCR), a partnership between the Australian Bureau of Meteorology (BoM) and the Commonwealth Scientific Industrial and Research Organisation (CSIRO), developed a long-term global wind-wave hindcast focused on the central and South Pacific (Durrant et al., 2013a, 2013b). It is an implementation of the third-generation spectral wind-wave model WAVEWATCH III® v4.08 (Tolman, 2009), forced with the Climate Forecast System Reanalysis (CFSR) 10 m winds and ice concentration (Saha et al. 2010) and its extension Climate Forecast System Version 2 (CFSv2). It provides hourly information of both integrated wave parameters and directional wave spectra around the globe, with higher resolution around Australia and the Pacific Islands. Regarding the model configuration, some of its most salient features are: the Ardhuin et al. (2010) source term parameterizations; the Discrete Interaction Approximation (DIA, Hasselmann et al. 1985) for non-linear wave-wave interactions; the third-order Ultimate Quickest propagation scheme (Leonard, 1979; 1991), including the garden sprinkler effect correction (Tolman, 2002); JONSWAP bottom friction, and Battjes and Janssen (1978) shallow water depth breaking. Besides, an increase of the sheltering term from 1.0 to 1.2 (related to an effective wind reduction by shorter waves) and decrease of the non-dimensional growth factor of the input source term (βmax) from 1.52 to 1.33 were implemented, which improved the wave model performance in the Southern Ocean. Integrated parameters derived from the hindcast have been

144 validated against observations and satellite data around the world, displaying a good
145 performance of the model in terms of bias and root mean square error, and since its release this
146 hindcast has been used in various wave studies (e.g., Gallop et al., 2014; Marshall et al., 2015,
147 2018; Rapizo et al., 2015). A comprehensive assessment of the skill of the CAWCR wave
148 hindcast can be found in Durrant et al. (2014) for the whole globe, and in Hemer et al. (2017)
149 for the Australian region, and therefore is omitted here.

150 The output of the CAWCR waves hindcast used in this study consists of hourly archives of
151 directional wave spectra for 312 locations around the world, with a spatial resolution of 10°.
152 The hindcast considers the varying sea ice concentrations, using the approach described by
153 Tolman (2003). Hence, there are high latitude grid points covered by ice during certain periods
154 of the year, where no wave information is available. In order to ease the calculations, these ice-
155 affected grid points were not considered in this analysis. The spectral frequencies in the model
156 are discretised in 29 bins, varying exponentially from 0.038 Hz (26 s period) to 0.5 Hz (2 s
157 period), and the directions were taken every 15°. Whilst the CAWCR hindcast spans from 1979
158 through to near present, the selected time interval for this study spans from January 1st, 1979
159 to December 31st, 2016.

160 **2.2 EOF analysis applied to directional wave spectral data**

161 In order to study the interannual variability of global directional wave spectra, an empirical
162 orthogonal function (EOF) analysis was performed to reduce the data in a meaningful way. The
163 EOF technique (e.g. Preisendorfer & Mobley, 1988) is commonly used in climate sciences to
164 find the main patterns of variability of a certain variable, how this pattern changes through
165 time, and the percentage of the total variance explained by these 'modes'. A common approach
166 is to perform the EOF analysis on gridded data of a scalar quantity that fluctuates in time to
167 find the geographic patterns that depict the main modes of variability of that quantity (e.g.

Deser et al., 2010; Gulev & Grigorieva, 2006; for wave-related studies, see Hemer et al., 2009 or Semedo et al., 2011). Here, following Echevarria et al. (2019), we employ a slightly different approach where the main modes of variability of the wave spectral density in the frequency/direction domain were obtained for each one of the spectral grid points of the model. These patterns represent the main modes of wave variability in the spectral domain and the methodology allows us to analyse their temporal variability independently.

First, daily averages of the wave spectra at each grid point were computed. The model wave spectrum is expressed as $S(f_i, \theta_j, x_p, t)$, with f_i the frequencies (i=1,…,29), θ_j the directions (j=1,…,24), x_p the locations (p=1,…,312) and t the times (each day from Jan 1st 1979 to Dec 31st 2016). The daily averages were applied across each frequency/direction grid point and for each location separately. The daily seasonal cycle was computed (and removed from the data) using the 1979-2016 average spectra for each day of the year (the average for the 29th of February was computed with the available 10 spectra only, but for the rest of the days 38 daily spectra were used to compute the average). Then, the data for each location were rearranged into a matrix containing the time series for each frequency/direction bin in the rows and each daily mean spectra in the columns (the dimensions of the matrix are 696 x 13880; 696 = 29 frequencies x 24 directions, and 13880 = no. of days in the time period selected). The covariance matrix was next computed, and the EOFs derived from it (see Echevarria et al. (2019) or Shimura and Mori (2019) for a more detailed description and application of this methodology).

2.3 The Pacific-South American (PSA) patterns and other climate indices

As explained earlier, the PSA patterns are defined as the second and third EOFs of the 500mb (or hPa) geopotential height (GPH) anomaly of the Southern Hemisphere, respectively (the first EOF corresponds to SAM). As such, they represent standing oscillations that are in

quadrature, and their indices describe the temporal variability of the amplitude of these oscillations. Daily PSA-1 and PSA-2 indices from January 1st 1979 to December 31st 2016 were constructed using 500mb GPH data taken from the NCEP/NCAR Reanalysis 1 (Kalnay et al., 1996). First, the PSA spatial patterns were computed as the second and third EOFs of the monthly averaged (instead of daily) 500mb GPH anomalies from 20°S to 70°S, after removing the seasonal cycle and weighing the data by the cosine of the latitude. Then, daily GPH anomalies were projected onto these patterns to obtain the daily PSA indices. These daily indices were normalized by the standard deviation of the monthly indices. The signs of the PSA patterns were taken as those in Mo and Higgins (1998).

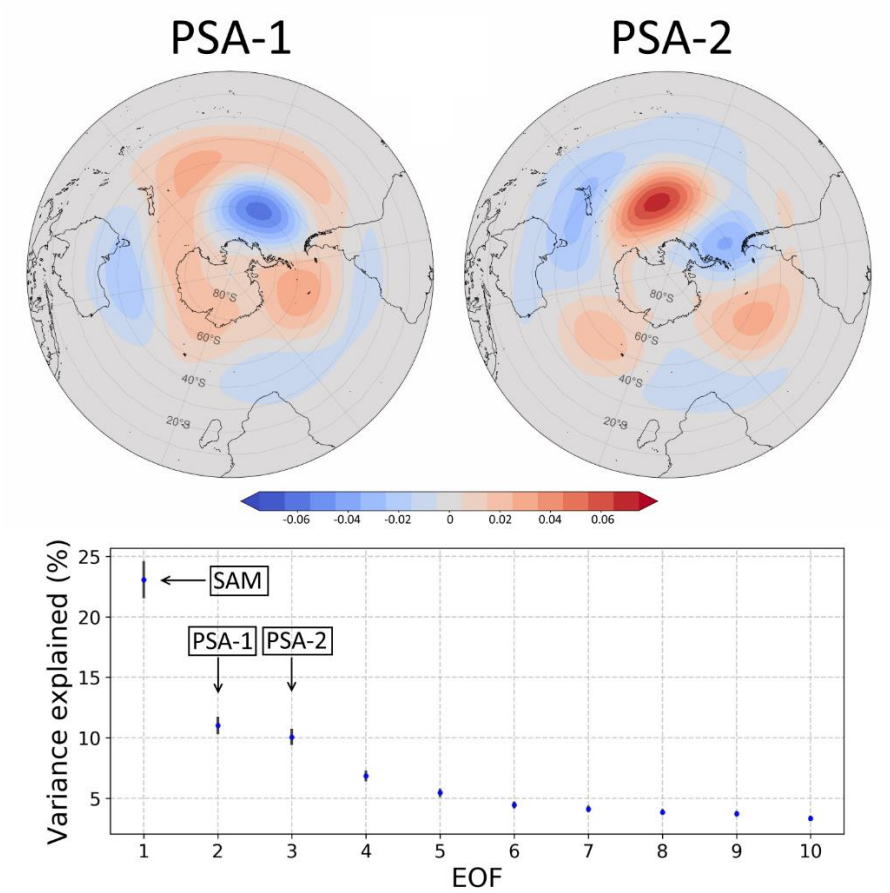

Figure 1. PSA-1 (top left) and PSA-2 (top right) patterns computed from monthly 500mb geopotential height anomalies from 20°S to 70°S. Units are carried in the Principal Component time series. The eigenvalue spectrum is shown in the bottom figure.

Other climate mode indices were also analysed in this study: These included indices of the Southern Annular Mode (SAM, Limpasuvan & Hartmann 1999), the Arctic Oscillation (AO, Thompson & Wallace 1998), the North Atlantic Oscillation (NAO, Wanner et al., 2001), the El Niño – Southern Oscillation (ENSO, Philander 1983) characterized by the NINO3.4 index, and the Pacific-North American mode (PNA, Wallace & Gutzler 1981). The SAM, AO, NAO and PNA daily indices from January 1st 1979 to December 31st 2016 and the NINO3.4 index from September 1st 1981 to December 31st 2016 were obtained from NOAA's Climate Prediction Center (http://www.cpc.ncep.noaa.gov).

3 Results

Daily mean spectra were computed for each day from 1st of January 1979 to 31st of December 2016 for each grid point, and the analysis described in Section 2.2 was carried out to extract the main patterns of spectral variability (EOFs) and their temporal evolution (Principal Components). For the interpretation of the results, it must be kept in mind that the reconstruction of the original spectral data from a few EOFs is achieved as follows:

$$Reconstructed\ spectra = \sum_i EOF_i * PC_i + S_{mean} \quad [1]$$

with PC being the Principal Component time series, i the number of EOFs selected and S_{mean} is the average spectra for each day of the year. Thereby, Section 3.1 presents maps of the first two EOFs (the most important spectral patterns of variability at each grid point), and Section 3.2 shows the variance explained by these two modes of variability, to determine how many EOFs should be taken to attain an accurate reconstruction of the original values. These sections, however, do not display information about the amplitude of the variability represented by the EOFs. Instead, the temporal information is contained in the Principal Component (PC) time series, which are described in Section 3.3. Once the spectral patterns of variability have been characterized, Section 3.4 describes how their variability is modulated by the PSA patterns.

Finally, for completion and as a corroboration of the methodology, in Section 3.4 other climate mode indices are analysed, for which their relationships to the wave climate have already been studied (namely, SAM, ENSO, AO, NAO and PNA).

3.1 Principal modes of interannual variability of the wave spectra

As described in Section 2.2, at each spectral grid point the dataset consisted of a sequence of daily mean directional wave spectra (from 1979 to 2016, with a total of 13880 days), and the EOFs represent the patterns of spectral variability that arise from that sequence. This methodology was previously applied by Echevarria et al. (2019) at the global scale and by Shimura and Mori (2019) around Japan. Both studies found two distinct main patterns of spectral variability, which were also identified in this study. They will be hereafter labelled as "swell mode" and "rotation mode". The former describes the intensification/reduction of a wave signal in the spectra, typically a low frequency one, and the latter characterizes a change in the direction of that wave signal (see Figures 4 and 7 of Echevarria et al. (2019) and Figure 10 of Shimura and Mori (2019)).

The patterns depicted in EOF-1 are predominantly swell modes, and the rotation modes are contained mostly in EOF-2 (although swell and rotation modes can also be found in higher-order EOFs). Figure 2 shows the global distribution of the swell modes. The red and blue tones correspond to EOF-1 and the orange tones to higher order EOFs that also represent a swell mode (this was corroborated by checking that the linear correlation of their PC time series with that of the neighbouring locations was statistically significant at the 99% confidence interval and higher than 0.3. Swell modes were identified up to EOF-10). At high latitudes of both hemispheres, these patterns show eastward propagating low frequency (swell) waves, which are a result of the westerly winds that blow in this area. The EOFs represent the variation in their intensity throughout the years, i.e., if the signal was constant in time, the EOF would not

capture it. It can be observed how these swell waves propagate toward lower latitudes following great circle paths, shown as orange and green lines in Figure 2. At high latitudes close to the wave generation area, the swell signals are broader, and once they disperse, they become more focused in one direction as they approach the equatorial regions. There is also a transition of the peak energy toward lower frequencies between the high-latitudes and equatorial waves, evidencing their dispersive behaviour.

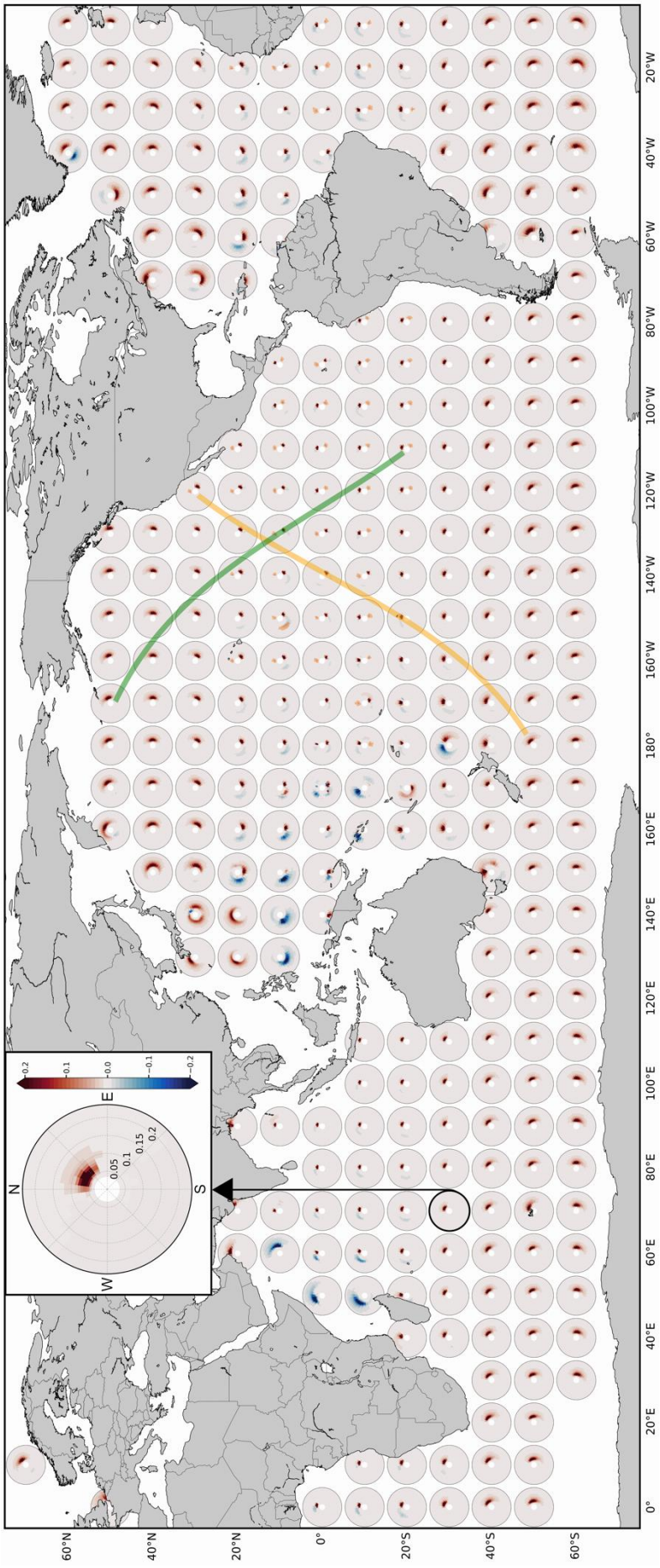

Figure 2. Principal modes of interannual spectra variability patterns (EOF-swell). The axis limits and the colorbar ranges are the same in every case and are shown for one location as reference. Directions are in oceanographic convention, i.e., the direction waves propagate to.

At low latitudes, particularly in the eastern Pacific, two swell modes were identified: namely, swell waves coming from the Southern Ocean and swell waves coming from the North Pacific. The variability of these two systems cannot be captured jointly in a single EOF; hence one swell mode is captured by EOF-1 and the other mode is obtained in higher order EOFs (labelled with orange tones in Figure 2). These are the primary and secondary swell components. Figure 2 shows that these swell waves can coexist in a band of latitudes of approximately ±20° around the equator. In the North Indian Ocean, a higher frequency signal in the spectra emerges as a result of the variability of the surface winds produced by the Asian Monsoon. There is also faint evidence of the influence of the trade winds in equatorial regions, generating a relatively high frequency signal in the spectra. The sign of these patterns (EOFs) is meaningless in itself; whether a given pattern represents a positive or negative anomaly depends on the sign of the product of the EOF pattern and its corresponding PC time series (see equation [1]).

Figure 3 shows the rotation modes, which are mostly captured in EOF-2. These patterns show positive and negative values at both sides of the main wave signal observed in the swell mode, representing a shift in spectral density from one direction to another. For example, in the North Pacific, most patterns in EOF-2 show negative values in the east direction and positive values in the southeast direction, which represents a clockwise rotation for positive values of the Principal Component. At low latitudes, two rotation modes can be observed, one for each swell component (the second rotation mode was selected only if the correlation between their PC time series and that of its neighbouring locations was statistically significant at the 99% confidence interval and higher than 0.3).

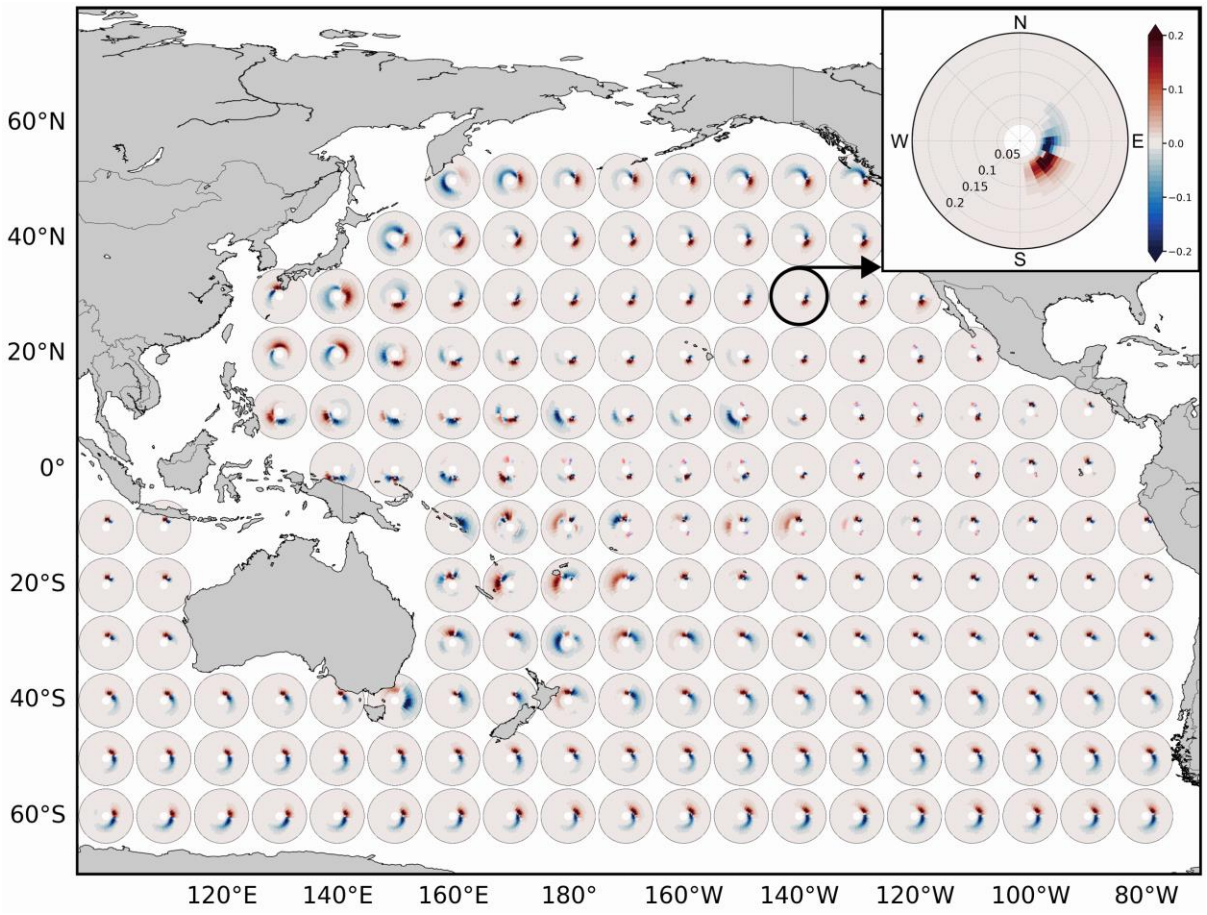

Figure 3. EOF-rotation patterns for the Pacific Ocean. Axis limits and colorbar range as in Figure 2.

3.2 Variance explained by swell and rotation modes

The variance explained by the swell and rotation mode at each grid point is an important parameter for assessing the accuracy of the reconstructed data (Figure 4). The regions where the swell mode explains the highest amount of variance are located at high latitudes, in the areas of most intense wave generation. It is greater than 50% in most areas of the Southern Ocean and the eastern North Pacific and Atlantic. It attains its lowest values in the equatorial regions and in the eastern sides of ocean basins. As to the variance explained by the rotation mode (Figure 4.b), areas with relatively high values are found southwest of Australia and in the east Atlantic. In total, the variance explained by both EOF modes together is more than 70% in the Southern Ocean, east Indian Ocean and North Pacific and Atlantic. On the other hand, in low latitude areas the variance explained by both EOFs is lower than 50%.

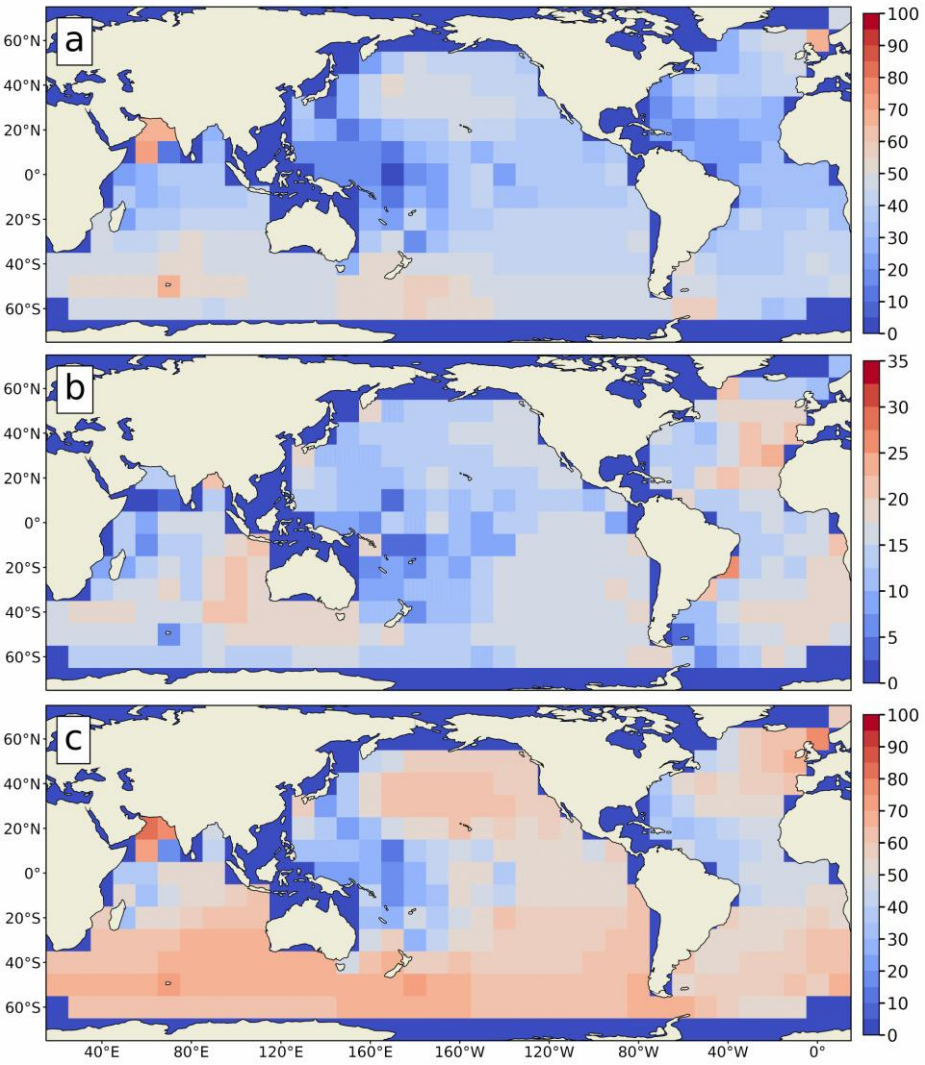

Figure 4. Variance explained by a) EOF-swell, b) EOF-rotation and c) EOF-swell and EOF-rotation together.

3.3 Amplitude of the Principal Component (PC) time series

The patterns of spectral variability depicted by the EOFs represent standing oscillations, and as such do not change shape with time, but they do change intensity; unseen in Figures 2 and 3. Instead, the PC time series describe the change in intensity of these patterns, daily and throughout the years. The standard deviation of these time series is taken as an indication of the waves' variability at each grid point, and its distribution is presented in Figure 5 (results are shown for the main swell mode, the variability of the rotation modes presents a similar

distribution, although with lower amplitude). In this way, considering equation [1], this information aids to better depict the temporal evolution of the patterns shown in Figure 2.

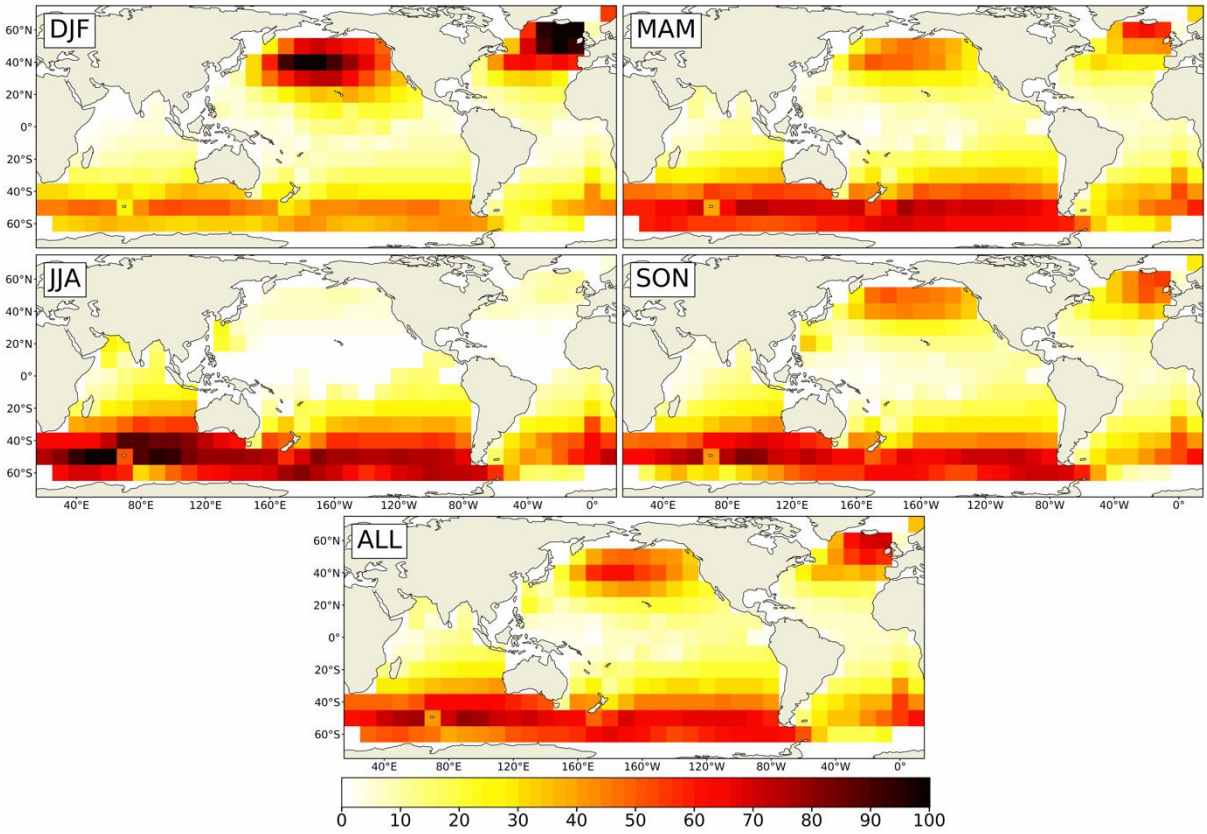

Figure 5. Distribution of the standard deviation of the first Principal Component time series, normalised so that the maximum value is 100.

The maximum variation (highest standard deviation) in the PC time series of the swell modes is found at high latitudes, especially in the North Atlantic during December-January-February (DJF) and in the South Indian Ocean in June-July-August (JJA), meaning that the patterns shown in Figure 2 oscillate with greater amplitude in these areas. On the other hand, the standard deviation decreases toward equatorial regions, meaning that the wave spectral variability is lowest there. That is, the absolute change in wave conditions is much smaller than at higher latitudes, consistent with the general decrease in mean zonal wind toward the equator. Accordingly, strong and significant wave signals can occur at high latitudes in connection with

326 tropical modes of atmospheric variability, via Rossby wave teleconnection to the extratropics
327 (e.g. Marshall et al. 2015, Marshall et al. 2018).

328 **3.4 Influence of the PSA patterns on the spectral wave climate**

329 The main aim of this work is to investigate the role that the PSA patterns have on the
330 interannual variability of the global wave climate, in this case described through daily
331 directional wave spectra. The temporal variability of the PSA patterns and the wave climate is
332 described in this case by the PSA index and the PC time series of the EOFs, respectively. First,
333 the PSA indices and PC time series (corresponding to the swell and rotation modes) at each
334 location were detrended and the Pearson's linear correlation between them was computed at
335 each grid point. In the equatorial regions, where there are two swell modes present, we chose
336 the mode corresponding to the Southern Ocean generated swell, since it was better correlated
337 with the PSA indices. Additionally, the daily mean significant wave height (Hs) was computed
338 using the original wave spectra at every grid point and its anomalies were also correlated to the
339 PSA indices to study the differences in both approaches. It should be noted that Hs is computed
340 by integrating the full wave spectrum over all frequencies and directions, hence it is
341 representative of the total wave energy contained in it, whereas the EOF patterns are
342 representative of a single wave system in the spectrum. The comparison with the PSA indices
343 is presented in Figure 6.

344

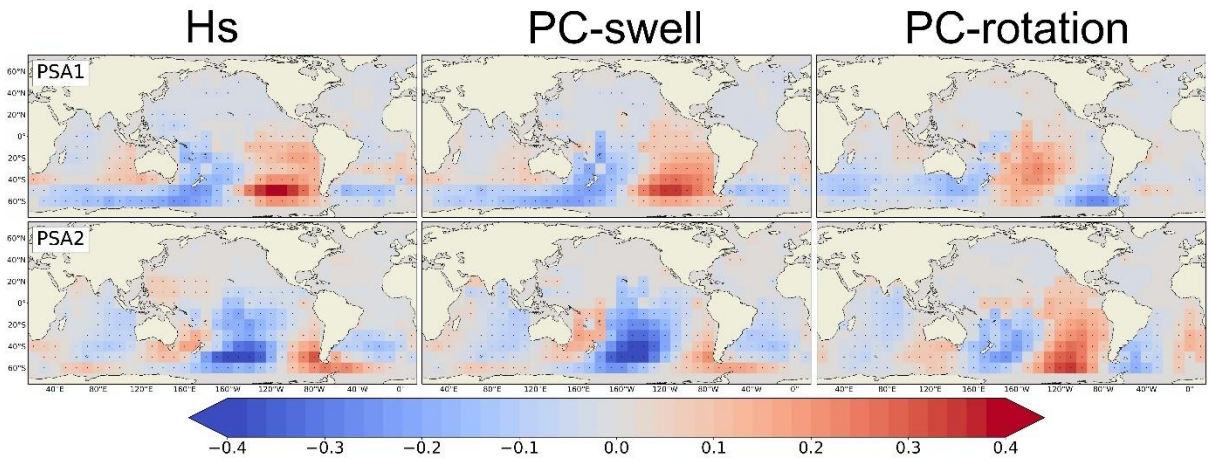

345

346 **Figure 6.** Upper panels: Correlation between the PSA-1 index and Hs (left), PC-swell (middle) and PC-
347 rotation (right). Lower panels: Correlation between PSA-2 index and Hs (left), PC-swell (middle) and
348 PC-rotation (right). Significant correlations at the 99% confidence level are marked with a black dot.

349 The patterns in Figure 6 show distinct (coherent) and statistically significant (α=0.01)
350 relationships between the PSA modes and the wave climate of the South Pacific. The influences
351 are primarily focused in the Southern Hemisphere, but also extend into the Northern
352 Hemisphere. The zonal wavenumber 3 feature that characterizes the PSA patterns can be
353 identified in the correlation patterns of Figure 6. The PSA-1 pattern is positively correlated
354 with wave heights in the eastern South Pacific extending to the equatorial regions, and
355 negatively correlated (although with less intensity) in the Tasman Sea and south of Australia.
356 There is also a positive, albeit very low, correlation off Western Australia and a negative
357 correlation in the South Atlantic. The PSA-1 also has an important apparent influence on the
358 waves' rotation in the South Pacific, as evidenced by its positive correlation with PC-rotation
359 in the central South Pacific and negative correlation south of Australia and Africa and south-
360 westward of Chile. Considering Figure 3, this means that an anticlockwise rotation would
361 develop in the central South Pacific, and a clockwise one around South Australia, South Africa
362 and Chile, during positive phases of PSA-1. The PSA-2 pattern, on the other hand, presents a
363 strong negative correlation with the wave heights in the central South Pacific, also extending

toward the equator. With less intensity, there is a negative correlation in the Indian and South Atlantic Ocean and a positive correlation in the Tasman Sea, and along the Chilean coast and Drake Passage. The PSA-2 would produce an anticlockwise rotation of the waves in the eastern sector of the South Pacific that appears to be more intense than the one generated by PSA-1 pattern, and an anti-clockwise rotation around New Zealand. All correlations described are statistically significant at the 99% confidence interval.

To further understand the nature of the relationship between the PSA patterns and the wave climate in the Southern Hemisphere, composite maps of wind anomalies during positive phases or stages of PSA-1 and PSA-2 were calculated, using daily mean 10 m wind data from the NCEP/NCAR I reanalysis. Figure 7 shows the mean wind velocity and direction for the period 1979-2016 (upper panel) and the deviations from that mean state (wind anomalies) during positive phases of PSA-1 (middle panel) and PSA-2 (lower panel). Positive and negative phases of PSA-1 or PSA-2 were defined as those times where the corresponding daily PSA index was higher than one standard deviation and lower than minus one standard deviation, respectively.

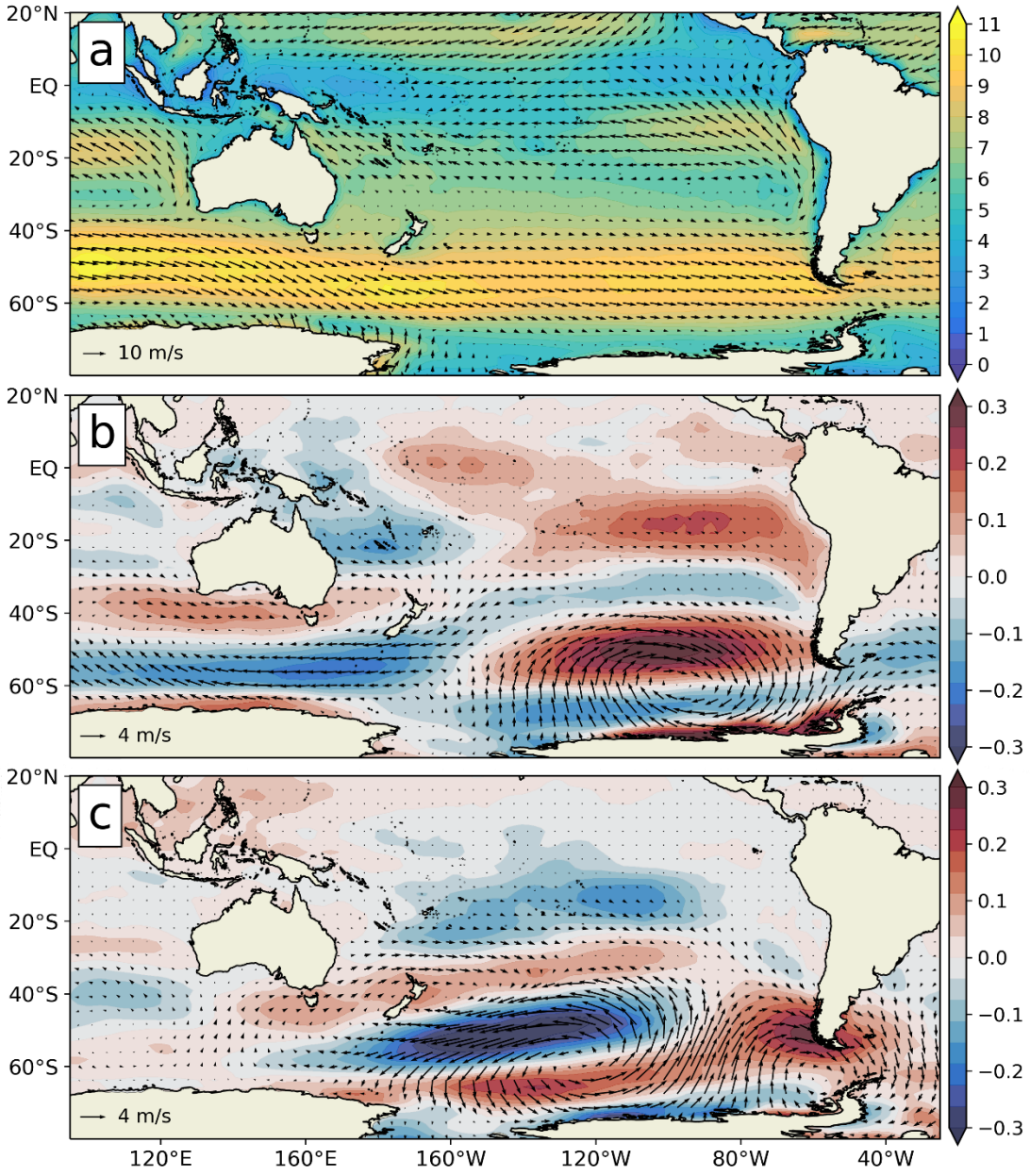

Figure 7. a) Mean wind vectors for the period 1979-2016 and mean wind velocity in colors. b) and c) Arrows: wind anomalies during positive phases of PSA-1 (a) and PSA-2 (b). Colors: correlation coefficient between daily mean wind intensity and PSA-1 (a) and PSA-2 (b) index for the period 1979-2016.

The surface wind anomalies during positive stages of PSA-1 and PSA-2 are mostly a response to the GPH anomalies that characterize them. During positive phases of PSA-1, a clockwise circulation pattern develops, with its center at approximately 60°S; 90°W, which strengthens the predominantly westerly winds between 40°S and 60°S and weakens the winds south of

60°S. PSA-1 also appears to exert some influence on the surface winds south of Australia and New Zealand. There is a mild positive correlation between the PSA-1 index and the wind intensity to the south-west of Australia, and a negative correlation south of ~45°S which acts to reduce the westerlies intensity in this area. On the other hand, the most conspicuous characteristic of positive stages of PSA-2 is an anticlockwise circulation anomaly centered at 60°S; 120°W. The associated composite negative zonal wind anomalies between 40°S and 60°S result in less intense westerlies in the South Pacific, as it is observed in the strong negative correlation between PSA-2 index and the wind intensity south-eastwards of New Zealand. Southward of 60°S, there is a positive zonal wind anomaly which extends to South America and strengthens near the southwest coast of Chile. This positive wind anomaly would translate into more intense wave heights in this area, as Figure 6 suggests.

3.5 Influence of other climate indices on the spectral wave climate

Finally, we also compared the PC time series of the two main patterns of spectral variability (swell and rotation modes) with other climate mode indices: SAM, AO, NAO, NINO3.4 and PNA. As before, both the PC and climate index were detrended prior to the analysis and the linear correlation coefficient between them was computed. For the equatorial regions, where there are two swell modes present, we selected the PC time series that best correlates with the climate index (for example, the SAM has a very strong relationship with the Southern Ocean generated swell, and therefore when correlating with the SAM index, the Southern Ocean swell mode was selected instead of the Northern Hemisphere generated swell). The correlation distribution for each climate mode index with Hs, PC-swell and PC-rotation is shown in Figure 8.

The SAM is the main driver of atmospheric variability in the Southern Hemisphere, influencing the strength and position of the westerly winds through changes in the pressure difference

411 between the Antarctic continent and mid-latitudes. There is a significant positive correlation
412 between the SAM index and the daily mean Hs anomalies at high latitudes of the Southern
413 Ocean and in the South Pacific, and negative correlations at mid-latitudes of the Atlantic and
414 Indian Ocean. The strongest relationship is found at high latitudes of the Southern Ocean,
415 southward of Australia and New Zealand. This is a consequence of shifts in the Southern
416 Hemisphere storm belt during positive SAM phases, which generate positive and negative
417 zonal wind anomalies at high and mid-latitudes, respectively. The maps of the correlation
418 coefficient between SAM and the Principal Component time series of the swell modes (PC-
419 swell) shows a similar distribution to that of Hs. However, the correlation with Hs decays
420 toward lower latitudes, whereas the correlation with PC-swell is maintained approximately in
421 the same values. This means that, at low latitudes, the SAM exerts its influence primarily on
422 the Southern Ocean generated swell depicted by EOF-swell. Since Hs is representative of the
423 total energy contained in the spectrum, it also considers high-frequency waves that are less
424 affected (or not affected at all) by the SAM, and that is the reason why the correlation values
425 between SAM and Hs are lower than those between SAM and PC-swell. This is also evident
426 in the Indian Ocean, where the correlation with Hs rapidly decays northward of 30°S while the
427 correlation with PC-swell remains significant all the way to the equator. The SAM also appears
428 to have widespread influence on the waves' rotation of the SH, especially southwest of
429 Australia, as evidenced by the positive correlation between the SAM index and PC-rotation
430 (the positive sign means that the rotation is anticlockwise for positive phases of SAM; see
431 Figure 3).

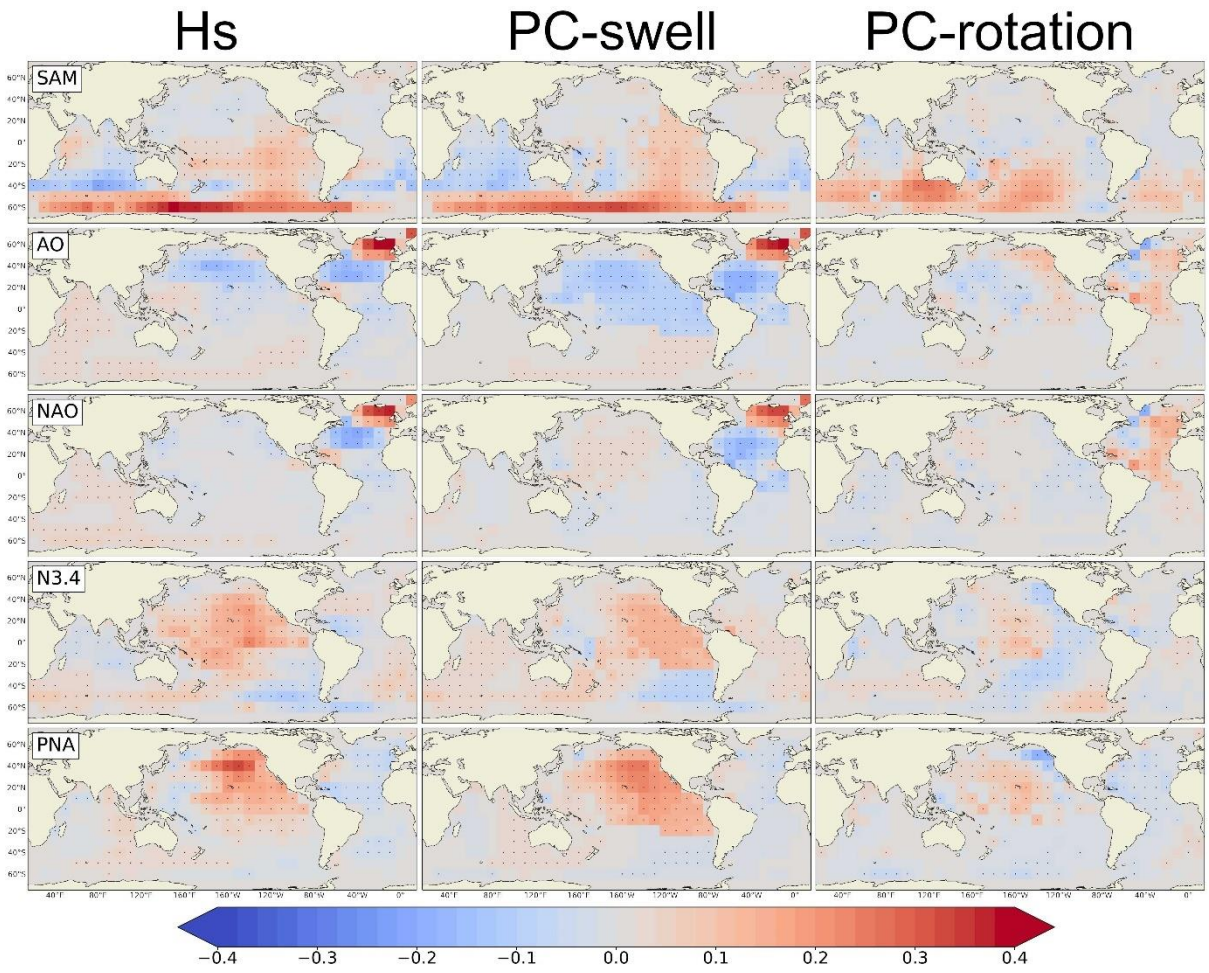

Figure 8. Distribution of the linear correlation coefficient between climate indices and the significant wave height (Hs) and PC-swell and PC-rotation. Significant correlations (at the 99% confidence level) are denoted with a black dot.

Likewise, the main driver of atmospheric variability in the Northern Hemisphere is its corresponding annular mode, the AO. Similar to the SAM, during positive phases of the AO, the westerly winds at high latitudes of the Northern Hemisphere contract toward the Arctic, producing a dipole of positive and negative zonal wind anomalies at high and mid latitudes, respectively. The strength and significance of the correlations between the AO index and PC-swell or Hs suggest that the atmospheric circulation anomalies developed as a consequence of the AO have an important influence on the wave climate of the Northern Hemisphere. Again, the correlation with Hs decreases toward lower latitudes while the correlation with PC-swell is

maintained in approximately the same values as far as the equatorial regions. In this case, the eastern equatorial EOF pattern that was selected corresponds to the North Pacific generated swell mode, since it is the one that better correlates with the AO index. The correlation values are higher in the Atlantic Ocean than in the Pacific. The AO is also significantly related to the rotation of the wave signal, although this relationship is not as strong as the influence of SAM on wave rotation. Specifically, positive phases of the AO would correspond to a clockwise rotation in the east north Pacific and in the North Atlantic, and an anticlockwise rotation in the west Pacific. The pattern of correlation with the NAO is similar to that with the AO but restricted to the Atlantic Ocean.

The relationship between ENSO and the wave field is complex across the Pacific Ocean and, to a lesser extent, in some areas of the Indian and Atlantic Ocean. During El Niño events (defined as prolonged periods of warm sea surface temperatures anomalies (>0.5°C) in the central equatorial Pacific, which correspond to positive NINO3.4 index values. See: https://www.cpc.ncep.noaa.gov/), the easterly trade winds weaken and contract to the eastern equatorial Pacific, accompanied by a warming and consequent low sea-level pressure anomaly in this area. Further, teleconnections related to ENSO produce changes in the atmospheric circulation all around the world. During El Niño events, there tends to be an amplification and extension of the westerlies of the North Pacific toward the east, which translate into more intense wave generation. This is evidenced in Figure 5 by the positive correlation between the NINO3.4 index and Hs (or PC-swell) in this area and extending to the eastern equatorial Pacific. On the other hand, during La Niña events (defined as prolonged periods of cool sea surface temperature anomalies in the central equatorial Pacific, which correspond to negative NINO3.4 index values), a positive zonal wind anomaly tends to develop in the southeast Pacific (a strengthening of the westerlies), which translates into more intense wave generation in that area.

Finally, our results also suggest that the PNA has widespread influence on the waves in the eastern and central North Pacific. Positives phases of the PNA are associated with a deepening of the Aleutian Low and a consequent intensification of the westerly winds of the North Pacific, which in turn produce anomalously higher waves. There is also a weak negative correlation in the North Atlantic, which is more evident in the Hs. As to the correlation with PC-rotation, it shows low negative values (although statistically significant) in the North Atlantic and positive values in the western and central North Pacific. This means that during positive PNA phases, there is an intensification of the mean swell signals at high latitudes of the Pacific Ocean accompanied by a clockwise rotation of those waves. The contrary happens in the North Atlantic but less markedly, that is, a reduction of the intensity and anticlockwise rotation of the eastward propagating waves.

4 Summary and Discussion

The approach outlined in Echevarria et al. (2019), and briefly described in Section 2.2, was implemented in the present study to investigate the patterns of wave spectral variability using daily averaged directional wave spectra from 1979–2016, taken from the CAWCR global wave hindcast dataset. The time evolution of these main patterns of spectral variability at each point was then compared to various climate mode indices to better understand the potential drivers of interannual variations in the global spectral wave climate. The motivation for using directional wave spectra as opposed to integrated parameters is founded on the potential loss of representativeness of the latter, as discussed by Portilla-Yandún (2018). In short, we found that the PSA modes have a very strong and statistically significant (at the 99% level) connection with the South Pacific wave climate, suggesting that these modes play a very important and influential role in the region's wave climate, including along the coasts of New Zealand and Chile. Further, this methodology allowed us to separate the impact of different climate modes on different patterns of spectral variability (swell and rotation modes).

494 At high latitudes of both hemispheres, the main mode of interannual daily wave spectral
495 variability (EOF-1) corresponds to the variation of relatively low frequency (period of ~15 s)
496 waves that propagate eastwards as a consequence of the intense westerly winds; these swell
497 waves propagate equatorward following great circle paths, becoming an important source of
498 interannual variability at mid- and low latitudes. The second most important mode of variability
499 (EOF-2) at high latitudes represents a rotation of the main swell signals, alternatively clockwise
500 and anticlockwise depending on the sign of their PC time series. Finally, EOF-3 describes a
501 change in frequency of the observed wave signals, from lower to higher frequencies or vice
502 versa depending on the sign of their PC (figures not shown). At low latitudes, the wave climate
503 is more complex and multi-modal: there is variability associated with swell waves coming from
504 both hemispheres, with different time evolutions. Since both swell modes cannot be captured
505 jointly in a single EOF, one mode is captured in EOF-1 and the other mode in higher-order
506 EOFs. Likewise, there are "rotation" modes for the Northern and Southern Hemisphere swell
507 modes, captured in EOF-2 and higher-order EOFs. To provide more clarity and consistency to
508 our results, we decided to group all the "swell" modes in Figure 2 and the "rotation" modes in
509 Figure 3. In addition, in the western Atlantic and Pacific Oceans, there is a higher frequency
510 wave signal – a consequence of the easterly winds – that varies out of phase with the high
511 latitude generated swell waves. In the central and eastern Pacific, higher frequency signals were
512 also observed in the higher order EOFs but were not considered in this work.

513 The variance explained by EOF-swell is large at high latitudes, in areas of intense wave
514 generation (Figure 4). The eigenvalue spectrum (the distribution of variance explained across
515 the EOFs) for these locations is very steep. That is, EOF-1 explains a significantly larger
516 proportion of the variance than the remaining EOFs (figures not shown). The variance
517 explained by the swell and rotation modes together is generally higher than 70% for latitudes
518 greater than 20°, except in the western side of ocean basins. In the equatorial region, the

519 variance explained by both modes reaches an average value of around 50%. The eigenvalue
520 spectrum of these areas is relatively flat, that is, the variance explained by the first few EOFs
521 is comparatively similar. Therefore, it should be considered that, in terms of data
522 reconstruction, a different degree of accuracy was achieved at each model grid point.

523 Of all the climate mode indices considered in this study, PSA-1 and -2 presented the highest
524 values of correlation with daily time series of Hs or PC-swell in the south Pacific region. It is
525 well known that the Southern Ocean generated swell waves can travel across the Pacific,
526 reaching as far as the coasts of Alaska (Munk & Snodgrass, 1957; Snodgrass et al., 1966; Gallet
527 & Young, 2014). Our results suggest that the PSA modes could substantially modulate the
528 generation of these swell waves. PSA-1 is positively correlated with the wave heights (as
529 represented by Hs or PC-swell) in the eastern South Pacific, and negatively correlated
530 (although with less intensity) with wave heights in the Tasman Sea and in the Indian Ocean
531 sector of the Southern Ocean. These correlations range approximately between ±0.4 as shown
532 in Figure 6; however, if the analysis is performed using monthly averaged spectra the
533 correlations exceed ±0.7. The changes in wave height are a response to the wind anomalies
534 associated with PSA-1 (Figure 7b). During positive phases of PSA-1, there is an intensification
535 of the westerly winds in the southeast Pacific sector between 40°S and 60°S and a weakening
536 of the westerlies south of Australia. PSA-2 is strongly negatively correlated with the wave
537 heights in the central South Pacific, reaching minimum values of <-0.4 (<-0.7 if working with
538 monthly data). During positive phases of PSA-2, an anticlockwise circulation anomaly
539 develops at (60°S; 120°W) which dampens the wind intensity in the South Pacific sector,
540 diminishing the wave climate intensity in this area and across the South Pacific.

541 A noteworthy benefit of utilising the approach described in Section 2.2 is that it allowed us to
542 obtain time series of changes in modelled wave direction (PC-rotation). Both PSA-1 and -2
543 appear to have a significant impact on the rotation of the waves in the Southern Ocean. Positive

phases of PSA-1 are correlated with clockwise rotations south and east of Australia and to the southwest of Chile, and anticlockwise rotations in the central Pacific. Likewise, positive phases of PSA-2 are correlated with clockwise rotations around New Zealand and intense anticlockwise rotations in the eastern South Pacific. The anticlockwise and clockwise wave rotations south of Australia (identified with PSA-1 and PSA-2 respectively) could modulate changes in wave direction at the coast and hence impact or trigger dynamic processes in the south Australia sandy beaches. Previous research has highlighted the influence of SAM and ENSO on the wave climate of the Tasman Sea (e.g., Ranasinghe et al., 2004; Goodwin 2005; Hemer et al., 2009; Harley et al., 2010). Our results show correlation values for the PSA mode indices of similar magnitude as the correlation values for NINO3.4 index for the Tasman Sea, suggesting that the PSA patterns are also important for the wave climate of this region. Therefore, these results could aid to better understand the governing physical processes that modulate the interannual variability of the wave climate in the Tasman Sea. The strong correlation values between PSA indices and PC-swell and PC-rotation in the South Pacific suggest that the wave climate at the coasts of New Zealand, Chile and Perú could be particularly affected by this climate mode. However, an assessment of observational wave records in these areas is necessary to confirm this relationship.

Various other climate modes were also considered in our analysis, and their relationship with the main modes of spectral variability (swell and rotation modes) was assessed:

1. The Southern Annular Mode (SAM) is the dominant mode of interannual variability of the wave climate of the Southern Hemisphere, being positively correlated with Hs at high latitudes of the Southern Ocean and in the South Pacific basin and negatively correlated in parts of the Indian and east Atlantic Oceans. The patterns of correlation are consistent with those found by Hemer et al. (2009), Izaguirre et al. (2011) and Marshall et al. (2018). The correlation with Hs decays toward the equator whereas the

569 correlation with PC-swell is maintained in approximately the same values, since PC-
570 swell represents the variability of only a portion of the spectrum while Hs is
571 representative of the full wave energy contained in it. With the approach used in this
572 study, we find that the influence of SAM extends toward the North Indian Ocean and
573 even reaches the coasts of Baja California (~20°N). Our study suggests the SAM
574 significantly influences the rotation of the wave field in extended areas of the Southern
575 Hemisphere, especially southwest of Australia. This rotation is anticlockwise for
576 positive phases of SAM, which agrees well with previous results found by Hemer et al.
577 (2009).

578 2. The corresponding annular mode of the Northern Hemisphere, the Arctic Oscillation
579 (AO; otherwise known as the Northern Annular Mode), shows an analogous pattern of
580 correlation. There is a widespread negative correlation with wave heights during its
581 positive phases, when the Northern Hemisphere storm belt contracts toward higher
582 latitudes, generating negative zonal wind anomalies at mid-latitudes. As before, the
583 correlation between Hs and AO decreases equatorward, given that the full directional
584 spectrum is being integrated to compute Hs, and the AO is suggested to have a bigger
585 influence on a determined part of the spectra (North Pacific swell waves dispersing
586 equatorward), as can be seen in the correlation with PC-swell. The North Atlantic
587 Oscillation (NAO) shows a very similar pattern of correlation, but restricted to the
588 North Atlantic Ocean only, and our results are in close agreement to those of previous
589 studies that investigated the influence of the NAO on North Atlantic wave variability
590 (e.g., Woolf et al., 2002; Semedo et al., 2011).

591 3. The correlation analysis with the NINO3.4 index indicates that ENSO is a major source
592 of the signature in interannual variability in the global wave climate, with the highest
593 influence not surprisingly in the Pacific Ocean, which is the centre of action for ENSO

dynamics. The distribution of the correlation coefficient between NINO3.4 and Hs agrees with that of previous studies (see, for example, Figure 3 of Izaguirre et al. (2011)). El Niño events (positive NINO3.4) correspond with an increase in Hs in the North Pacific and in high latitudes of the Indian Ocean. During La Niña (negative NINO3.4), an increase of the wave height occurs in the southeast Pacific sector. There are some discrepancies between the Hs and PC-swell correlation distributions. For example, in the eastern equatorial Pacific, EOF-swell was selected as the mode that better correlates with the NINO3.4 index, which turned out to be the North Pacific swell. In the western equatorial Pacific, EOF-swell explains a relatively low percentage of the variance and that could be the reason for the differences with Hs in this area. As to the correlation between the NINO3.4 index and PC-rotation, it is positive in the western and southeast Pacific and negative in large areas of the eastern Pacific. This implies that El Niño events would produce a clockwise rotation of the main wave signal in most of the eastern Pacific Ocean and an anticlockwise rotation in the west. However, the correlation, although statistically significant, is generally very low with values around 0.25.

4. The Pacific-North American mode (PNA) has a significant impact on the wave climate of the North Pacific: it is correlated (R~0.3) with swell waves that are generated there and travel equatorward. The approach used in this study allows to infer that the PNA could influence the swell wave climate of the eastern equatorial Pacific. In fact, all the above-mentioned climate mode patterns appear to play respective roles in contributing to the interannual wave variability in the eastern equatorial Pacific region.

In summary, the methodology presented in this work agrees well with previous studies while at the same time allows us to better assess the potential influence of various climate modes on the components of the wave spectrum. It also helped us to better understand

619 which of these climate patterns apparently affect the changes in wave direction (rotation).
620 The PSA modes, previously not considered, seem to play a remarkably important
621 influential role in the wave climate of the South Pacific, governing major changes in wave
622 height and direction.

623 **Acknowledgements**

624 The authors acknowledge the availability of the CAWCR wave hindcast, funded through
625 the Australian Government Pacific-Australia Climate Change Science and Adaptation
626 Program. The CAWCR hindcast data is available at http://data-
627 cbr.csiro.au/thredds/catalog/catch_all/CMAR_CAWCR-
628 Wave_archive/CAWCR_Wave_Hindcast_1979-2010/catalog.html and http://data-
629 cbr.csiro.au/thredds/catalog/catch_all/CMAR_CAWCR-
630 Wave_archive/CAWCR_Wave_Hindcast_Jun_2013_-_Jul_2014/catalog.html. EE is
631 supported by funding from the UTAS-CSIRO Quantitative Marine Science Program, the
632 Institute for Marine and Antarctic Studies, the Australian Research Council Centre of
633 Excellence for Climate Extremes and a CSIRO Office of the Chief Executive top-up
634 scholarship. MH is supported by the Australian Government National Environmental
635 Science Program Earth Systems and Climate Change (NESP ESCC) Hub. NJH
636 acknowledges support from the Australian Research Council Centre of Excellence for
637 Climate Extremes (Grant CE170100023) and also the NESP ESCC Hub.

638 **References**

639 Ardhuin, F., Rogers, E., Babanin, A. V., Filipot, J. F., Magne, R., Roland, A., ... & Collard,
640 F. (2010). Semiempirical dissipation source functions for ocean waves. Part I: Definition,
641 calibration, and validation. *Journal of Physical Oceanography*, 40(9), 1917-1941.
642 https://doi.org/10.1175/2010JPO4324.1

643 Battjes, J. A., & Janssen, J. P. F. M. (1978). Energy loss and set-up due to breaking of
644 random waves. *Coastal Engineering*, 1978, pp. 569-587.
645 https://doi.org/10.1061/9780872621909.034

646 Deser, C., Alexander, M. A., Xie, S. P., & Phillips, A. S. (2010). Sea surface temperature
647 variability: Patterns and mechanisms. *Annual review of marine science*, 2, 115-143.
648 https://doi.org/10.1146/annurev-marine-120408-151453

649 Durrant, T., Hemer, M., Trenham, C., & Greenslade, D. (2013a). CAWCR Wave Hindcast
650 1979–2010 v7. Data Collection, CSIRO. http://dx.doi.org/10.4225/08/523168703DCC5

651 Durrant, T., Hemer, M., Trenham, C., & Greensdale, D. (2013b). CAWCR wave Hindcast
652 extension Jan 2011-May 2013. v4. Data Collection, CSIRO.
653 https://doi.org/10.4225/08/52817E2858340

654 Durrant, T., Greenslade, D., Hemer, M., & Trenham, C. (2014). A global wave hindcast
655 focused on the Central and South Pacific (Technical Report No. 070) The Centre for
656 Australian Weather and Climate Research.

657 Echevarria, E. R., Hemer, M. A., & Holbrook, N. J. (2019). Seasonal Variability of the
658 Global Spectral Wind Wave Climate. *Journal of Geophysical Research: Oceans*, 124(4),
659 2924-2939. https://doi.org/10.1029/2018JC014620

660 Gallet, B., & Young, W. R. (2014). Refraction of swell by surface currents. *Journal of*
661 *marine research*, 72(2), 105-126. https://doi.org/10.1357/002224014813758959

662 Gallop, S. L., Young, I. R., Ranasinghe, R., Durrant, T. H., & Haigh, I. D. (2014). The
663 large-scale influence of the Great Barrier Reef matrix on wave attenuation. *Coral Reefs*,
664 33(4), 1167-1178. https://doi.org/10.1007/s00338-014-1205-7

665 Goodwin, I. D. (2005). A mid-shelf, mean wave direction climatology for southeastern
666 Australia, and its relationship to the El Niño—Southern Oscillation since 1878 AD.
667 *International Journal of Climatology*, 25(13), 1715-1729. https://doi.org/10.1002/joc.1207

668 Gulev, S. K., & Grigorieva, V. (2006). Variability of the winter wind waves and swell in
669 the North Atlantic and North Pacific as revealed by the voluntary observing ship data.
670 *Journal of Climate*, 19(21), 5667-5685. https://doi.org/10.1175/JCLI3936.1

671 Harley, M. D., Turner, I. L., Short, A. D., & Ranasinghe, R. (2010). Interannual variability
672 and controls of the Sydney wave climate. *International Journal of Climatology*, 30(9),
673 1322-1335. https://doi.org/10.1002/joc.1962

674 Hasselmann, S., Hasselmann, K., Allender, J. H., & Barnett, T. P. (1985). Computations
675 and parameterizations of the nonlinear energy transfer in a gravity-wave spectrum. Part II:
676 Parameterizations of the nonlinear energy transfer for application in wave models. *Journal*
677 *of Physical Oceanography*, 15(11), 1378-1391. https://doi.org/10.1175/1520-
678 0485(1985)015<1378:CAPOTN>2.0.CO;2

679 Hegermiller, C. A., Antolinez, J. A., Rueda, A., Camus, P., Perez, J., Erikson, L. H., ... &
680 Mendez, F. J. (2017). A multimodal wave spectrum–based approach for statistical
681 downscaling of local wave climate. *Journal of Physical Oceanography*, 47(2), 375-386.
682 https://doi.org/10.1175/JPO-D-16-0191.1

683 Hemer, M. A., Church, J. A., & Hunter, J. R. (2009). Variability and trends in the
684 directional wave climate of the Southern Hemisphere. *International Journal of*
685 *Climatology*, 30(4), 475-491. https://doi.org/10.1002/joc.1900

686 Hemer, M. A., Zieger, S., Durrant, T., O'Grady, J., Hoeke, R. K., McInnes, K. L., &
687 Rosebrock, U. (2017). A revised assessment of Australia's national wave energy resource.
688 *Renewable Energy*, 114, 85-107. https://doi.org/10.1016/j.renene.2016.08.039

689 Izaguirre, C., Méndez, F. J., Menéndez, M., & Losada, I. J. (2011). Global extreme wave
690 height variability based on satellite data. *Geophysical Research Letters*, 38(10).
691 https://doi.org/10.1029/2011GL047302

692 Kalnay, E., Kanamitsu, M., Kistler, R., Collins, W., Deaven, D., Gandin, L., ... & Zhu, Y.
693 (1996). The NCEP/NCAR 40-year reanalysis project. *Bulletin of the American*
694 *meteorological Society*, 77(3), 437-472. https://doi.org/10.1175/1520-
695 0477(1996)077<0437:TNYRP>2.0.CO;2

696 Leonard, B. P. (1979). A stable and accurate convective modelling procedure based on
697 quadratic upstream interpolation. *Computer methods in applied mechanics and*
698 *engineering*, 19(1), 59-98. https://doi.org/10.1016/0045-7825(79)90034-3

699 Leonard, B. P. (1991). The ULTIMATE conservative difference scheme applied to
700 unsteady one-dimensional advection. *Computer methods in applied mechanics and*
701 *engineering*, 88(1), 17-74. https://doi.org/10.1016/0045-7825(91)90232-U

702 Limpasuvan, V., & Hartmann, D. L. (1999). Eddies and the annular modes of climate
703 variability. *Geophysical Research Letters*, 26(20), 3133-3136.
704 https://doi.org/10.1029/1999GL010478

705 Marshall, G. J., & Thompson, D. W. (2016). The signatures of large-scale patterns of
706 atmospheric variability in Antarctic surface temperatures. *Journal of Geophysical*
707 *Research: Atmospheres*, 121(7), 3276-3289. https://doi.org/10.1002/2015JD024665

708 Marshall, G. J., Thompson, D. W., & Broeke, M. R. (2017). The signature of Southern
709 Hemisphere atmospheric circulation patterns in Antarctic precipitation. *Geophysical*
710 *research letters*, 44(22). https://doi.org/10.1002/2017GL075998

711 Marshall, A. G., Hendon, H. H., Durrant, T. H., & Hemer, M. A. (2015). Madden Julian
712 Oscillation impacts on global ocean surface waves. *Ocean Modelling*, 96, 136-147.
713 https://doi.org/10.1016/j.ocemod.2015.06.002

714 Marshall, A. G., Hemer, M. A., Hendon, H. H., & McInnes, K. L. (2018). Southern annular
715 mode impacts on global ocean surface waves. *Ocean Modelling*, 129, 58-74.
716 https://doi.org/10.1016/j.ocemod.2018.07.007

717 Marshall, A. G., Hemer, M. A., & McInnes, K. L. (2020). Australian blocking impacts on
718 ocean surface waves. *Climate Dynamics*, 54, 1281-1294. https://doi.org/10.1007/s00382-
719 019-05058-8

720 Mo, K. C., & Ghil, M. (1987). Statistics and dynamics of persistent anomalies. *Journal of*
721 *the Atmospheric Sciences*, 44(5), 877-902. https://doi.org/10.1175/1520-
722 0469(1987)044<0877:SADOPA>2.0.CO;2

723 Mo, K. C., & Higgins, R. W. (1998). The Pacific–South American modes and tropical
724 convection during the Southern Hemisphere winter. *Monthly Weather Review*, 126(6),
725 1581-1596. https://doi.org/10.1175/1520-0493(1998)126<1581:TPSAMA>2.0.CO;2

726 Mo, K. C., & Paegle, J. N. (2001). The Pacific–South American modes and their
727 downstream effects. *International Journal of Climatology: A Journal of the Royal*
728 *Meteorological Society*, 21(10), 1211-1229. https://doi.org/10.1002/joc.685

729 Munk, W. H., & Snodgrass, F. E. (1957). Measurements of southern swell at Guadalupe
730 Island. *Deep Sea Research*, 4, 272-286. https://doi.org/10.1016/0146-6313(56)90061-2

731 Philander, S. G. H. (1983). El Nino southern oscillation phenomena. *Nature*, 302(5906),
732 295-301. https://doi.org/10.1038/302295a0

733 Portilla-Yandún, J., Salazar, A., & Cavaleri, L. (2016). Climate patterns derived from ocean
734 wave spectra. *Geophysical Research Letters*, 43(22).
735 https://doi.org/10.1002/2016GL071419

736 Portilla-Yandún, J. (2018). The global signature of ocean wave spectra. *Geophysical*
737 *Research Letters*, 45(1), 267-276. https://doi.org/10.1002/2017GL076431

738 Preisendorfer, R. W., & Mobley, C. D. (1988). Principal component analysis in
739 meteorology and oceanography (Vol. 425). Amsterdam: Elsevier.

740 Ranasinghe, R., McLoughlin, R., Short, A., & Symonds, G. (2004). The Southern
741 Oscillation Index, wave climate, and beach rotation. *Marine Geology*, 204(3-4), 273-287.
742 https://doi.org/10.1016/S0025-3227(04)00002-7

743 Rapizo, H., Babanin, A. V., Schulz, E., Hemer, M. A., & Durrant, T. H. (2015). Observation
744 of wind-waves from a moored buoy in the Southern Ocean. *Ocean Dynamics*, 65(9-10),
745 1275-1288. https://doi.org/10.1007/s10236-015-0873-3

746 Renwick, J. A., & Revell, M. J. (1999). Blocking over the South Pacific and Rossby wave
747 propagation. *Monthly Weather Review*, 127(10), 2233-2247. https://doi.org/10.1175/1520-
748 0493(1999)127<2233:BOTSPA>2.0.CO;2

749 Saha, S., Moorthi, S., Pan, H. L., Wu, X., Wang, J., Nadiga, S. et al. (2010). The NCEP
750 climate forecast system reanalysis. *Bulletin of the American Meteorological Society*, 91(8),
751 1015-1057. https://doi.org/10.1175/2010BAMS3001.1

752 Semedo, A., Sušelj, K., Rutgersson, A., & Sterl, A. (2011). A global view on the wind sea
753 and swell climate and variability from ERA-40. *Journal of Climate*, 24(5), 1461-1479.
754 https://doi.org/10.1175/2010JCLI3718.1

Shimura, T., Mori, N., & Mase, H. (2013). Ocean waves and teleconnection patterns in the Northern Hemisphere. *Journal of Climate*, 26(21), 8654-8670. https://doi.org/10.1175/JCLI-D-12-00397.1

Shimura, T., & Mori, N. (2019). High-resolution wave climate hindcast around Japan and its spectral representation. *Coastal Engineering*, 151, 1-9. https://doi.org/10.1016/j.coastaleng.2019.04.013

Snodgrass, F. E., Hasselmann, K. F., Miller, G. R., Munk, W. H., & Powers, W. H. (1966). Propagation of ocean swell across the Pacific. *Philosophical Transactions of the Royal Society of London. Series A, Mathematical and Physical Sciences*, 259(1103), 431-497. https://doi.org/10.1098/rsta.1966.0022

Stopa, J. E., Cheung, K. F., Tolman, H. L., & Chawla, A. (2013). Patterns and cycles in the climate forecast system reanalysis wind and wave data. *Ocean Modelling*, 70, 207-220. https://doi.org/10.1016/j.ocemod.2012.10.005

Thompson, D. W., & Wallace, J. M. (1998). The Arctic Oscillation signature in the wintertime geopotential height and temperature fields. *Geophysical research letters*, 25(9), 1297-1300. https://doi.org/10.1029/98GL00950

Tolman, H. L. (2002). Alleviating the garden sprinkler effect in wind wave models. *Ocean Modelling*, 4(3-4), 269-289. https://doi.org/10.1016/S1463-5003(02)00004-5

Tolman, H. L. (2003). Treatment of unresolved islands and ice in wind wave models. *Ocean Modelling*, 5(3), 219-231. https://doi.org/10.1016/S1463-5003(02)00040-9

Tolman, H. L. (2009). User manual and system documentation of WAVEWATCH III TM version 3.14 (Technical note No. 276). NOAA/NWS/NCEP/MMAB.

777 Wallace, J. M., & Gutzler, D. S. (1981). Teleconnections in the geopotential height field
778 during the Northern Hemisphere winter. *Monthly Weather Review*, 109(4), 784-812.
779 https://doi.org/10.1175/1520-0493(1981)109<0784:TITGHF>2.0.CO;2

780 Wanner, H., Brönnimann, S., Casty, C., Gyalistras, D., Luterbacher, J., Schmutz, C., ... &
781 Xoplaki, E. (2001). North Atlantic Oscillation–concepts and studies. *Surveys in geophysics*,
782 22(4), 321-381. https://doi.org/10.1023/A:1014217317898

783 Woolf, D. K., Challenor, P. G., & Cotton, P. D. (2002). Variability and predictability of the
784 North Atlantic wave climate. *Journal of Geophysical Research: Oceans*, 107(C10).
785 https://doi.org/10.1029/2001JC001124

786 Young, I. R. (1999). Seasonal variability of the global ocean wind and wave climate.
787 *International Journal of Climatology*, 19(9), 931-950. https://doi.org/10.1002/(SICI)1097-
788 0088(199907)19:9<931::AID-JOC412>3.0.CO;2-O